Journal of Applied Electrochemistry **34**: 119–125, 2004.

Effects of ceric ammonium nitrate (CAN) additive in HNO_3 solution on the electrochemical behaviour of ruthenium for CMP processes

W.-J. LEE[1,*], H.-S. PARK[2], S.-I. LEE[2] and H.-C. SOHN[2]
[1]*Corrosion Research Center, Department of Chemical Engineering and Materials Science, University of Minnesota, Minneapolis, MN 55455, USA*
[2]*Advanced Process Department 4, Memory Research & Development Division, Hynix Semiconductor, Inc., San 136-1 Ami-Ri, Ichon-Si, Kyunggi-Do 467-701, Korea*
*(*author for correspondence, e-mail: sambong@cems.umn.edu, woojin.lee@hynix.com)*

Received 27 May 2002; accepted in revised form 11 August 2003

Key words: ceric ammonium nitrate, chemical mechanical polishing, galvanic corrosion, ruthenium

Abstract

In order to develop a new chemical mechanical polishing process for ruthenium (Ru), the present work deals with the effect of a ceric ammonium nitrate (CAN) additive on the electrochemical behaviour of physical vapour deposited Ru films in a 1 M HNO_3 solution employing electrochemical methods and surface analytical techniques. By adding CAN to HNO_3 solution, the polarisation curves showed an increase in the corrosion potential and current, suggesting that Ru is anodically polarised by CAN as an oxidising additive. To characterise the influence of CAN, open-circuit potential (OCP) and potentiostatic anodic current transient curves were examined in CAN-containing HNO_3 solution and the resulting surfaces were then characterised by scanning electron microscopy and X-ray photoelectron spectroscopy. It is proposed that Ru is oxidised to heterogeneous Ru_2O_3 and RuO_2 films on the Ru surface in CAN-containing HNO_3 solution and galvanic corrosion occurs at grain boundaries, caused by the difference in OCP between the grain interiors and boundaries. The grain boundaries are oxidised to RuO_4, a volatile species, resulting in a roughened and porous structure.

1. Introduction

Ruthenium (Ru) films have recently attracted attention as a bottom electrode for capacitors in next-generation devices, such as a dynamic random access memory with a metal–insulator–metal capacitor using Ta_2O_5 or $(Ba,Sr)TiO_3$[BST], $SrTiO_3$[STO]. The Ru films can be easily patterned and have high electronic conductivity [1–3]. The technological interest has led to studies such as those by Saito and Kuramasu [4] who reported the excellent dry etching properties of Ru.

However, the high hardness and chemical inertness that make Ru attractive as an electrode material also present unique challenges when it is subjected to wet processes such as wet-etching and chemical mechanical polishing (CMP) [5]. Recently, Bilakhiya et al. [6] have employed a ceric ammonium nitrate $[Ce(NH_4)_2Ce(NO_3)_6]$ (CAN) solution dissolved in HNO_3 in order to oxidise Ru with cerium(IV) (Ce^{4+}) ions. Moreover, our preliminary results have revealed a series of electrolytes with varying chemistries suitable for Ru CMP as summarised in Table 1. Since there has been no previous report of a Ru wet-etching solution and a Ru cleaning or CMP technology, the present paper addresses these subjects.

Thus, we have elucidated the effect of CAN additives in 1 M HNO_3 on the electrochemical behaviour of physical vapour deposited (PVD) Ru film by using potentiodynamic polarisation experiments, open-circuit potential (OCP) and potentiostatic anodic current transient techniques, coupled with scanning electron microscopy (SEM) and X-ray photoelectron spectroscopy (XPS). From the experimental results, a viable model for PVD Ru dissolution in CAN-containing HNO_3 solutions is proposed. In this dissolution model, we take account of the OCP difference between the grain interiors and boundaries on a reacting Ru surface because the two regions behave differently in the strong oxidising conditions.

2. Experimental

PVD Ru films of 1000 Å thickness were sputtered at 300 °C in an Ar atmosphere of 3×10^{-3} Torr onto blanket silicon (Si) wafers using a 550 Å TiN/Ti

Table 1. Change in the removal rate obtained from the PVD- and CVD-Ru films with various electrolytes containing CAN

Various Electrolytes (wt.%)	PVD-Ru /Å min^{-1}	CVD-Ru /Å min^{-1}
0.22%HNO_3 + 0.66%CAN	2100	–
2%HNO_3 + 2%CAN	1845	600
6%HNO_3 + 2%CAN	1987	630
2%HCl + 2%CAN	933	1044
6%H_2SO_4 + 0.66%CAN	243	108
6%HNO_3 + 4%CAN	959	2316

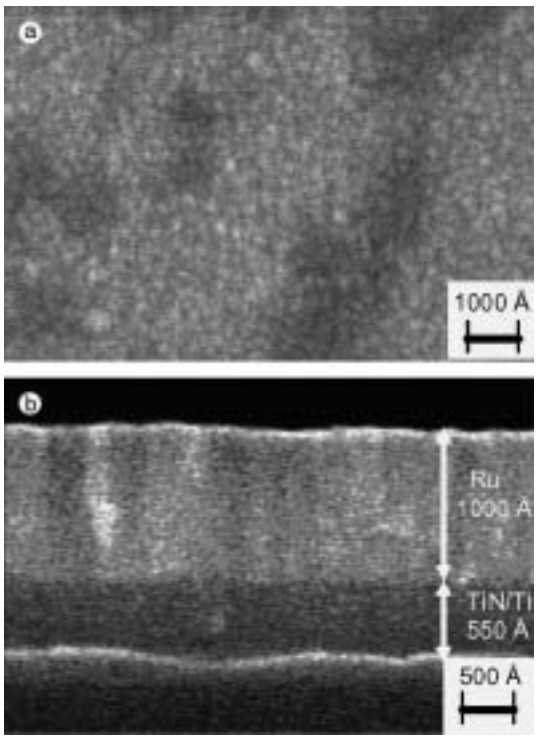

Fig. 1. (a) Top view and (b) cross-sectional view of SEM micrographs obtained from the PVD Ru thin film deposited on TiN/Ti/Si wafer.

adhesion layer. The unpolished Ru-deposited wafers were diced into 50 × 50 mm^2 samples. Figure 1a and b shows the top and cross-sectional SEM micrographs of the Ru/TiN/Ti film on the Si wafer samples. In all the electrochemical experiments, a platinum (Pt) mesh and an Ag/AgCl electrode were used as the counter and reference electrodes, respectively. All potentials are referred to the Ag/AgCl. The electrolytes used were 1 M HNO_3 solutions (pH = 1) containing CAN concentrations of 0 and 0.05 M. All the experiments were conducted at ambient temperature.

To compare the general electrochemical behaviour of PVD Ru in HNO_3 solutions with the two concentrations of CAN, potentiodynamic polarisation experiments were conducted on the PVD Ru film at a scan rate of 1 mV s^{-1} using an EG&G Model 273 Potentiostat/Galvanostat. OCP and potentiostatic anodic currents were measured with time on the Ru film at the corrosion potential E_{corr} and at potentials of +1.40, +1.50 and +1.60 V, respectively: the latter potentials were imposed by jumping the potential from OCP. After the potentiostatic current transient experiment, the surface morphology of each sample was carefully observed using SEM micrographs.

XPS (Quantum 2000) was carried out on Ru samples after immersion and anodic polarisation in CAN-containing HNO_3 solutions. The samples were excited by a monochromated Al anode X-ray source, AlK_α. The binding energy was measured against the Fermi level $3d_{5/2}$ Ag 367.9 eV. XPS spectra were acquired by recording the total electron current vs kinetic energy in a computer system. Spectra covering the binding energy range from 0 to 1400 eV were recorded to determine the constitutive elements of the respective surface films. Based on the detected elements, narrow spectra of Ru were recorded for certain energies. Depth analyses were also achieved with Ar^+ ion sputtering at 3.0 kV and 6 μA cm^{-1}. Alternate sputtering and spectrum collection were used to determine the change in concentration of each element at different depths in the surface film. The sputter rate relative to SiO_2 under identified conditions was approximately 35.7 Å min^{-1}.

3. Results and discussion

Figure 2 shows potentiodynamic polarisation curves obtained from the PVD Ru thin film in 1 M HNO_3 solutions with (0.05 M concentration) and without CAN at a scan rate of 1 mV s^{-1}. The anodic current density i_a in CAN-free HNO_3 solution showed a linear increase up to approximately +1.20 V with increasing potential, which is due to the formation of Ru_2O_3 and its

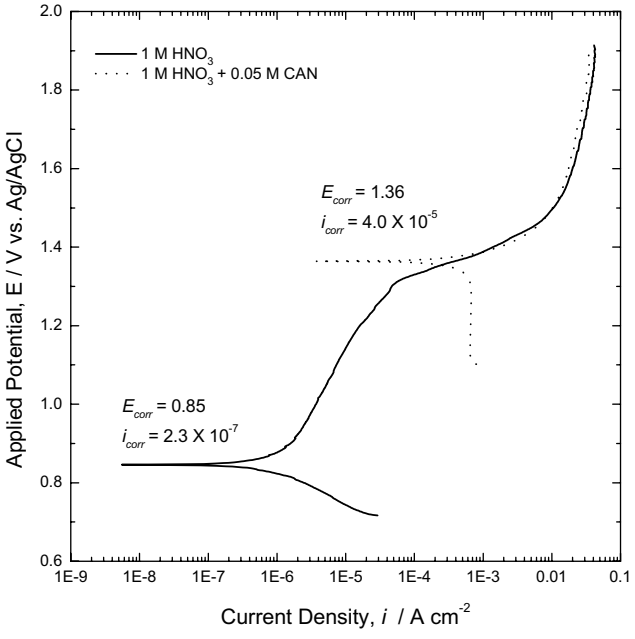

Fig. 2. Potentiodynamic polarisation curves of the PVD Ru thin film sample with a scan rate of 1 mV s^{-1} in: ——, 1 M HNO_3; -----, 0.05 M CAN + 1 M HNO_3 solutions.

conversion to rather stable RuO_2 according to the following Equations [7]

$$2Ru+3H_2O = Ru_2O_3 + 6H^+ + 6e^- \quad E = 0.541 - 0.0591\ pH \tag{1}$$

$$Ru_2O_3+H_2O = 2RuO_2 + 2H^+ + 2e^- \quad E = 0.740 - 0.0591\ pH \tag{2}$$

Then, i_a rose noticeably to a limiting rate corresponding to the commencement of oxygen evolution and vigorous corrosion to produce volatile RuO_4 at potentials above +1.20 V as [7]:

$$2H_2O = O_2 + 4H^+ + 4e^- \quad E = 1.03 - 0.0591\ pH \tag{3}$$

$$RuO_2 + 2H_2O = RuO_4 + 4H^+ + 4e^- \quad E = 1.19 - 0.0591\ pH \tag{4}$$

The values of the corrosion current density i_{corr} were shifted from 2.3×10^{-7} A cm^{-2} in the absence of CAN to higher values of 4.0×10^{-5} A cm^{-2} in the presence of 0.05 M CAN in HNO_3 solution. Also, the E_{corr} value suddenly increased from +0.85 to +1.36 V with addition of 0.05 M CAN to the HNO_3 solution. This is attributable to the enhanced oxidation of Ru by the spontaneous reduction of Ce^{4+} to Ce^{3+} ions at potentials above +1.24 V in CAN-containing HNO_3 solution as shown in the following reaction [7].

$$Ce^{4+} + e^- = Ce^{3+} \quad E = 1.24 - 0.0591\ pH \tag{5}$$

3.1. *Electrochemical behaviour of PVD Ru at steady state in CAN-containing nitric acid*

Figure 3 presents the OCP transient obtained from a PVD Ru film immersed for 40 000 s in the 1 M HNO_3

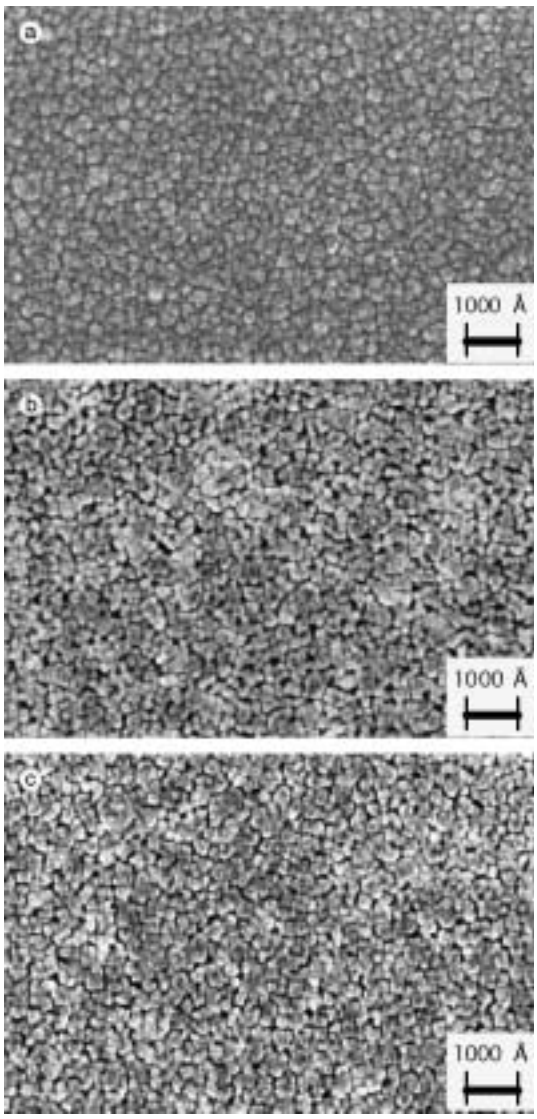

Fig. 4. SEM micrographs of surface morphology of the PVD Ru thin film sample after the OCP transient experiment in 0.05 M CAN + 1 M HNO_3 solution during (a) 5000 s (b) 10 000 s and (c) 40 000 s.

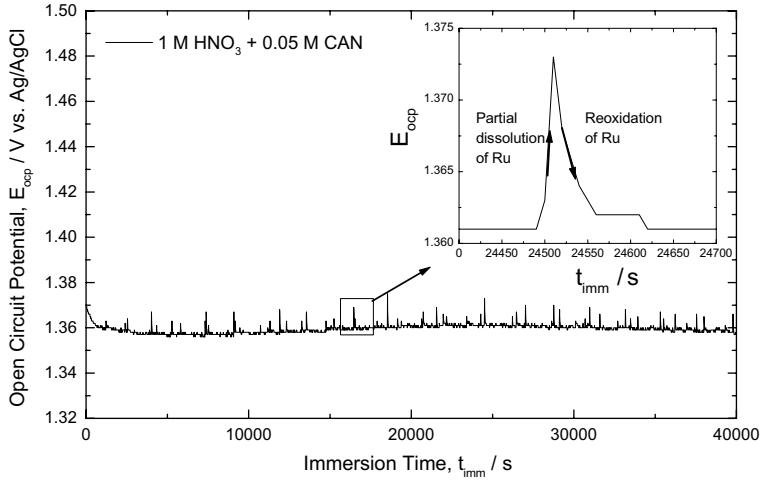

Fig. 3. Change in OCP with time, for the PVD Ru thin film sample during 40 000 s immersion in 0.05 M CAN + 1 M HNO_3 solution.

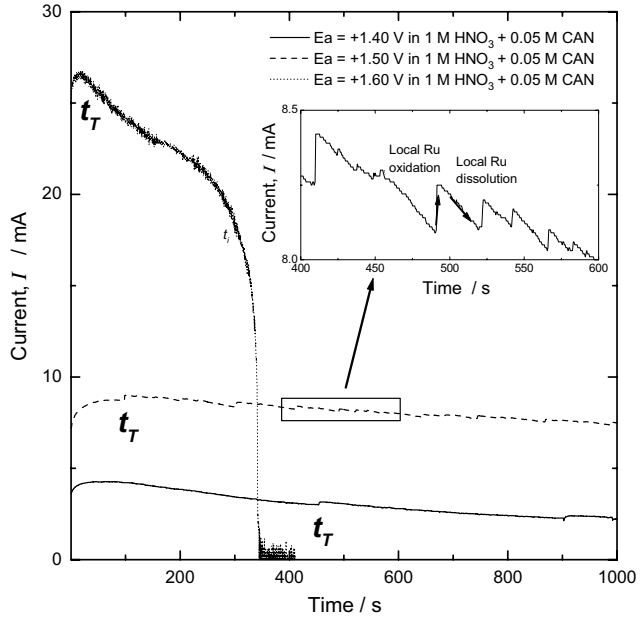

Fig. 5. Plots of anodic current I_a against time t on a linear scale for the PVD Ru thin film sample in 0.05 M CAN + 1 M HNO_3 solution, by jumping the OCP to various applied anodic potentials of: ——, +1.40 V; - - - - -, +1.50 V; ·····, +1.60 V.

solution with 0.05 M CAN. The OCP has an almost constant value of +1.36 V. However, superimposed on the constant baseline are multiple transients with an instantaneous jump and a subsequent drop in the OCP to near the baseline. The transient jump is presumably due to partial dissolution of the oxide film and subsequent reoxidation of Ru.

Figure 4a–c gives SEM micrographs of PVD Ru films exposed to the 0.05 M CAN-containing 1 M HNO_3 solution for immersion times of 5000, 10 000 and 40 000 s. Compared with the surface of the as-deposited Ru film of Figure 1a, it is seen that the surface morphology of the PVD Ru film immersed in CAN-containing solution has changed considerably. Interconnected globules and granules have formed with well pronounced boundaries. According to Equations 1 and 2, the granular surface is believed to be a Ru_2O_3 or RuO_2 layer deposited spontaneously on the Ru surface just after immersion in this solution. The layer appears is black in colour when examined under an optical microscope.

Furthermore, the boundaries between the grains appeared to be preferentially attacked with longer immersion time. Recognising that the grain boundaries are generally more susceptible to aggressive ion attack than the grain interiors due to their imperfect structure, it is proposed that the grain interiors become cathodic and the defective grain boundaries become anodic in this solution. As a result, galvanic corrosion occurs from a local cell established on the Ru surface. Accordingly, the PVD Ru film evolves to a granular structure after immersion in the CAN-containing solution.

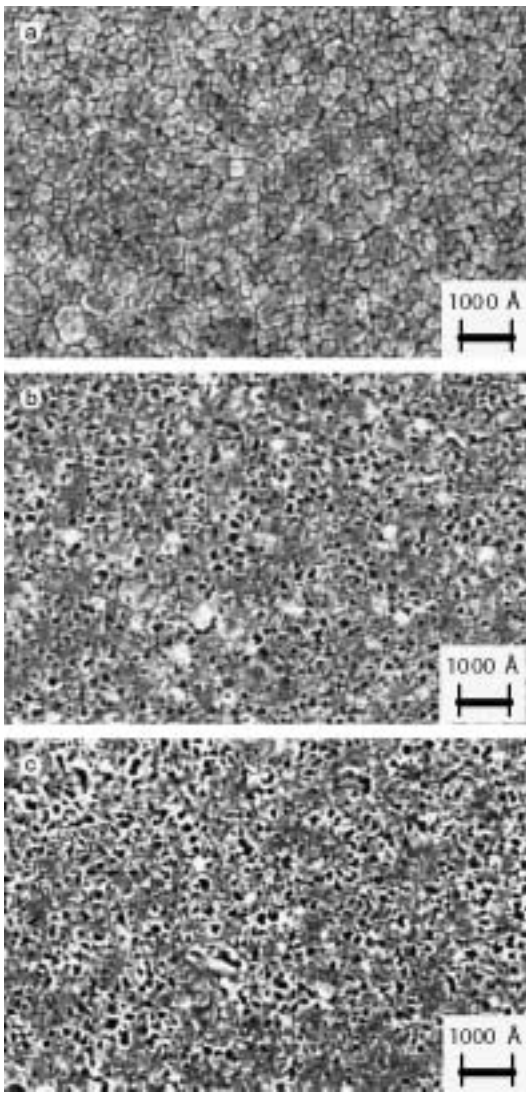

Fig. 6. SEM micrographs of surface morphology of the PVD Ru thin film samples after the anodic current transient experiment at +1.50 V in 0.05 M CAN + 1 M HNO_3 solution during (a) 60 s (b) 500 s and (c) 1000 s.

3.2. *Electrochemical behaviour of PVD Ru in CAN-containing nitric acid*

Figure 5 depicts potentiostatic anodic current I_a transients on a linear scale obtained from the PVD Ru thin film, measured at applied anodic potentials of +1.40, +1.50 and +1.60 V for 1000 s in 0.05 M CAN-containing HNO_3 solution. The transient curves showed a two-stage variation. There was a rapid rise in current up to the transition time t_T in the first period (*I*), followed by a slow decrease of the i_a value in the second period (*II*) to near zero current, respectively.

It should be noted that I_a in period *I* rose sharply as the applied potential increased. The increased current due to reactions (1), (2) and (4) is caused by an increase in the active area of the Ru conductive film. From the current decay in period *II* of the transient curve, it can be concluded that the active area of the Ru oxide film started to decrease due to oxide formation that reduced

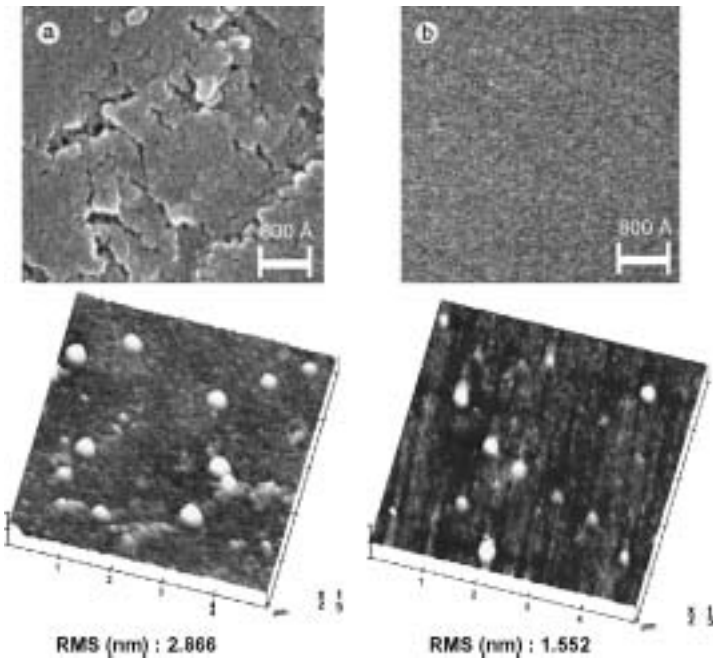

Fig. 7. AFM images obtained from the PVD Ru thin film samples (a) before and (b) after CMP in 0.05 M CAN + 1 M HNO_3 solution.

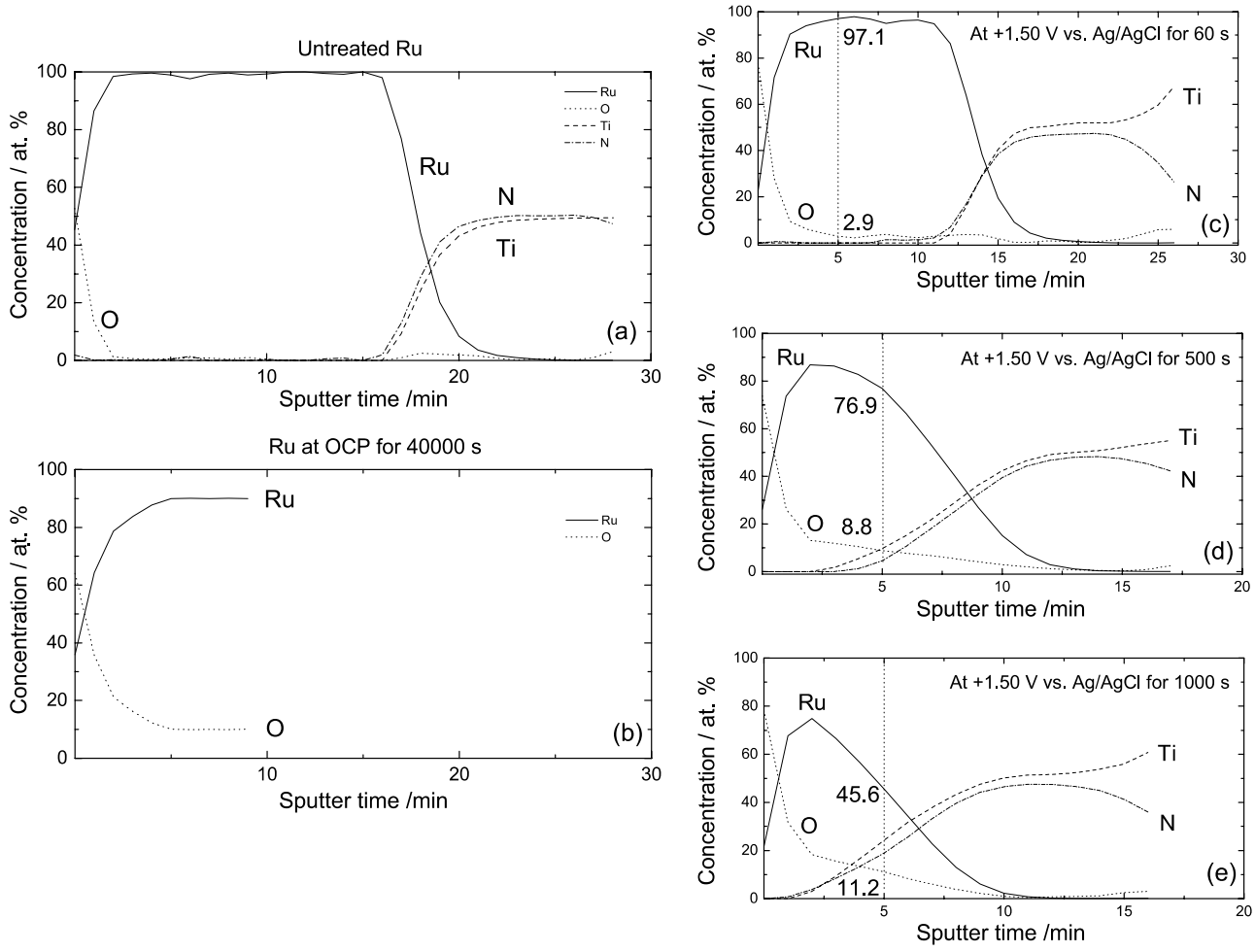

Fig. 8. XPS depth profile curves of the PVD Ru thin film samples with the CAN treatment during (a) 0 s and (b) 40 000 s at OCP, and (c) 60 s, (d) 500 s and (e) 1000 s at +1.50 V.

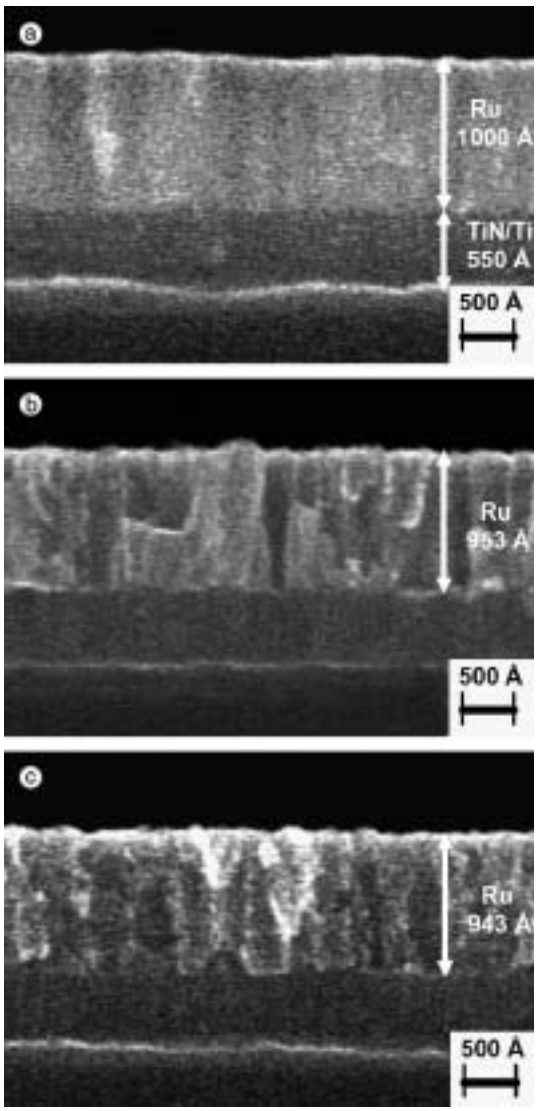

Fig. 9. Cross-sectional views of SEM micrographs of the PVD Ru thin film samples after the anodic current transient experiment at +1.50 V in 0.05 M CAN + 1 M HNO_3 solution during (a) 0 s (b) 60 s and (c) 1000 s.

the active area for dissolution. This was visually validated from the gradual brown colouration of the solution [8].

Moreover, the I_a value oscillated with a small amplitude in the period *II* after t_T. This signifies the local variation of the electrochemically accessible area, originating from the competition between anodic dissolution and formation of oxide on the Ru surface. We speculate that t_T can be considered as the initial time to dissolve out imperfections along the grain boundaries, and oxide formation processes begin to dominate the behaviour.

Figure 6a–c shows SEM micrographs of PVD Ru films subjected to an applied potential of +1.50 V for times of 60, 500 and 1000 s in 1 M HNO_3 solution with 0.05 M CAN. It was found that the PVD Ru film with 60 s polarisation below t_T had a granular structure, while those with 500 and 1000 s polarisation (above t_T) exhibited a highly porous structure. This implies pore formation on the Ru oxide surface, i.e., loss of active

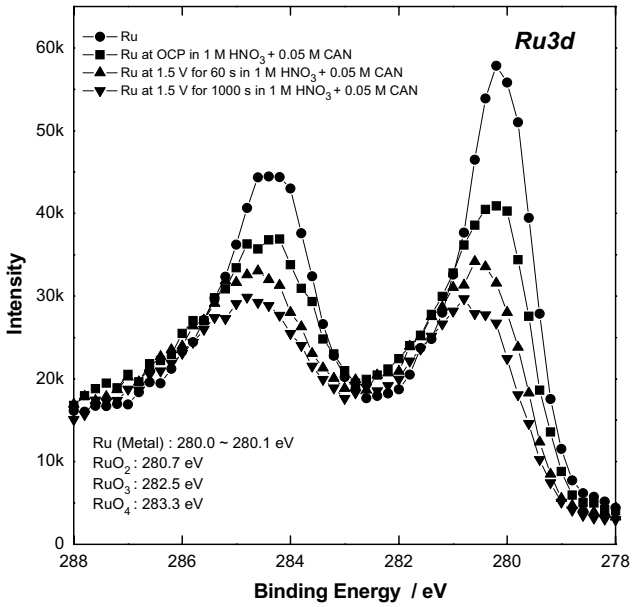

Fig. 10. XPS spectra of Ru 3d line for the PVD Ru thin film samples exposed to 0.05 M CAN + 1 M HNO_3 solution with various immersion times of: ●, 0 s; ■, 40 000 s at OCP; ▲, 60 s at +1.50 V; ▼, 1000 s at +1.50 V.

area by electrochemically accelerated grain boundary attack.

Figure 7a and b shows AFM images of the Ru film exposed to 0.05 M CAN-containing 1 M HNO_3 solution before and after CMP, respectively. It was found that a highly inert noble Ru film is evenly polished using this solution. This is supported by the lowered surface roughness value of 2.87–1.55.

XPS depth profiles obtained from the CAN-treated PVD Ru film samples with durations of 0, 40 000 s at OCP, and 60, 500 and 1000 s at +1.50 V are depicted in Figure 8a–e. The atomic concentration was estimated qualitatively as shown in the XPS profiles. From Figure 8a and b, it is remarkable that after the CAN treatment at OCP, oxygen atoms had diffused into the Ru, indicating that the Ru layer is partly oxidised near the outer surface.

Moreover, the Ru and O contents obtained after 5 min sputtering were diminished with increasing polarisation time from 97.1 to 45.6 at.% and raised from 2.9 to 11.2 at.%, respectively. At the same time, the Ti and N peaks corresponding to the TiN/Ti layer underneath showed up at the sample surface when an anodic potential of +1.50 V was applied. From the overall shape of the XPS curves for the chemically and electrochemically CAN-treated Ru, it is likely that the Ru oxide, formed just after the immersion in CAN-containing HNO_3, grows simultaneously with the selective dissolution in the progress of the polarisation time. This was well substantiated from the cross-sectional SEM view for the samples.

Cross-sectional SEM micrographs of the bare Ru and electrochemically treated Ru thin film samples after treatment times of 0, 60 and 1000 s in CAN-containing

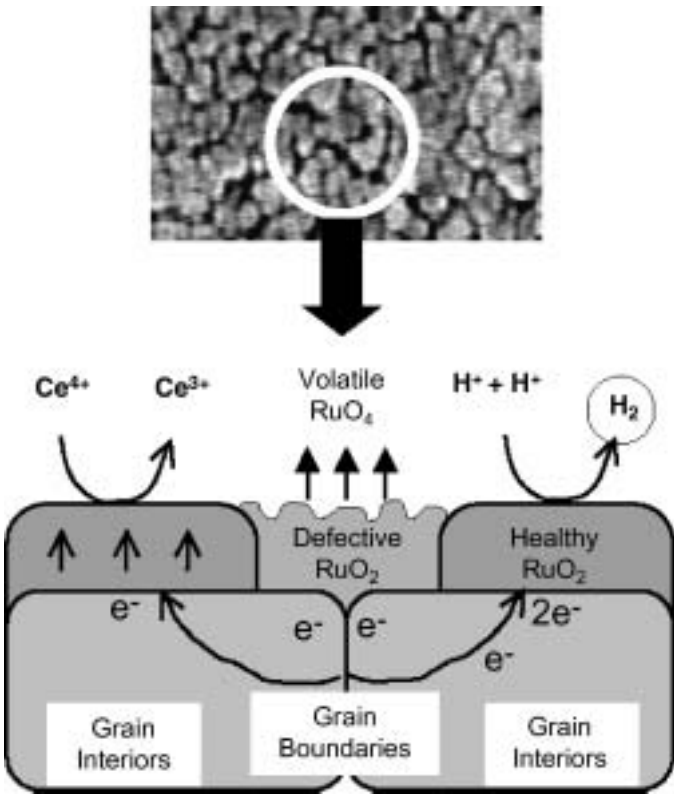

Fig. 11. Schematic diagram for the dissolution mechanism of Ru exposed to 0.05 M CAN + 1 M HNO_3 solution, proposed in this study.

HNO_3 solution, are illustrated in Figure 9a–c, respectively. Compared with the bare Ru, the electrochemically treated Ru samples showed a columnar structure of 30 nm in diameter as demonstrated in Figure 8b and c. This apparent columnar structure might result from selective anodic dissolution with concurrent oxide film formation in the dissolved region [8].

XPS spectra of the Ru 3d region, obtained from the PVD Ru film samples treated at various conditions in 0.05 M CAN-containing 1 M HNO_3 solution are exhibited in Figure 10. Here, the Ru $3d_{5/2}$ and Ru $3d_{3/2}$ binding energies for the CAN-untreated sample were initially found at 280.1 and 284.4 eV, respectively. These binding energies agreed with the data found in [9] for metallic Ru. However, after the chemical and electrochemical CAN-treatments, these signals became reduced and were shifted, with the scans reaching 280.6 and 284.6 eV at the end of the analysis, which presumably correspond to the stable RuO_2 film [10].

Consequently, it is proposed that the PVD Ru thin film could be efficiently oxidised with CAN addition to 1 M HNO_3 solution by the following mechanism: first, a Ru_2O_3 film is formed preferentially at grain interiors and boundaries on the Ru surface, and then is oxidised to the more stable RuO_2 with a roughened surface just after the immersion into CAN-containing HNO_3. Second, the Ru film undergoes galvanic corrosion generated from the difference in OCP values between the healthy RuO_2-covered grain interiors and the defective RuO_2-covered grain boundaries, leading to a granular morphology. Then, the grain boundaries are further oxidised to a volatile RuO_4 species, which leads to a roughened and porous structure. This model is schematically summarised in Figure 11.

Acknowledgements

The authors are grateful to Professor William. H. Smyrl, University of Minnesota, for his great help in improving this manuscript.

References

1. K. Kishiro, N. Inoue, S.C. Chen and M. Yoshimaru, *Jpn. J. Appl. Phys.* **37** (1998) 1336.
2. T. Aoyama, S. Yamazaki and K. Imai, *J. Electrochem. Soc.* **145** (1998) 2961.
3. J. Lin, N. Masaaki, A. Tsukune and M. Yamada, *Appl. Phys. Lett.* **74** (1999) 2370.
4. S. Saito and K. Kuramasu, *Jpn. J. Appl. Phys., Part 1* **31** (1992) 135.
5. K. Moeggenborg, V. Brusic, I. Cherian, A. Navarro-Powell and W. Downing, *in* Proceedings of Sixth International Chemical-Mechanical Planarisation for ULSI Multilevel Interconnection Conference, Santa Clara, CA, (2001) p. 150.
6. A.K. Bilakhiya, B. Tyagi and P. Paul, *Polyhedron* **19** (2000) 1233.
7. M. Pourbaix, *in* 'Atlas of Electrochemical Equilibria in Aqueous Solution' (Pergamon Press, GB, 1966).
8. V. Birss, R. Myers, H. Angerstein-Kozlowska and B.E. Conway, *J. Electrochem. Soc.* **131** (1984) 1502.
9. J.F. Mudler, W.F. Stickle, P.E. Sobol and K.D. Bomben, *in* 'Handbook of X-ray Photoelectron Spectroscopy' (Physical Electronics Inc., Minnesota, 1995).
10. M. Blouin and D. Guay, *J. Electrochem. Soc.* **144** (1997) 573.